Chapter 3

Design of surface plasmon resonance based on both side polished photonic crystal fiber for highly efficient refractive index sensor

In this chapter, we have designed and simulated both sides flat PCF polished with the plasmonic material layer of gold and an adhesive layer of TiO_2 over the flat surface. With optimized structural parameters, this PCF sensor provides maximum wavelength sensitivity for the analyte range of RI $n_a = 1.30 - 1.40$ *and maximum amplitude sensitivity for RI* $n_a = 1.39$. *The proposed sensor structure has improved results then to previous chapter in the manner of maximum wavelength sensitivity, amplitude sensitivity, and sensor resolution. Fabrication through the stack and draw method has been described in this chapter. The prime application of this sensor structure is cancer cell detection, and other than this, it has applications in different fields, such as biomedical and biochemical field*

Chapter 3: A both side polished PCF sensor

3.1 Introduction

Surface plasmon resonance (SPR) based sensing technology has achieved a solitary place due to its reliability and higher sensing results. Collective oscillation of free electrons for the incident electromagnetic wave at the interface of dielectric and metal is called surface plasmon oscillation, and quanta of these oscillations are known as surface plasmon wave (SPW). The propagation constant (K_{SP}) of SPW is calculated by Maxwell's equation that remains continuous throughout the metal-dielectric (M/D) interface. Lightwave (p-polarized) incident at metal-prism interface in Kresthmann's configuration at angle more than critical angle generates wave called evanescent wave that decay exponentially along dielectric near metal [88]. Such evanescent wave has propagation constant (K_{ev}) and can interact with SPW. Surface plasmon wave propagation constant (K_{SP}) and evanescent wave propagation constant (K_{ev}) matches at particular wavelength known as resonance wavelength [88]. In the field of optoelectronic, some devices like Silicon-based photonic chips provide favorable and optimistic results with this technology [119]. The SPR sensor also has some other application areas such as biomolecular analyte detection, biosensor, environmental protection, and food safety [120] [121], . Experimental verification of SPR sensors has also been reported for gas detection using the Kresthmann's method [121]. But such a conventional prism-based SPR sensor is costly and bulky in size, limiting the performance of remote sensing and other applications [122]. Miniaturization is a critical factor to overcome such a problem, and optical fiber plays an important role in his due to its small size and flexibility. These conventional optical fibers are mechanically stable as well as provide low confinement loss in the visible range. Although conventional fiber is better for sensing, it has less freedom of tuning parameters to improve the performance [123].

In order to overcome this snag in conventional fiber, various research has been performed on photonic crystal fiber (PCF) based SPR sensors due to their compact size, lightweight, tuning optical parameters property, which make these sensors attractive and can be used efficiently for sensing applications [124]. Such PCF-based sensors provide better sensitivity and less confinement loss than other conventional fiber sensors [90]. We can use two kinds of PCF structures, which are based on the plasmonic layer coating method. In the first method, a plasmonic layer is coated inside the PCF air holes called internal sensing [73] [91]. Several researchers have been worked on this mechanism [74] [125] [73]. S. Selvendran's structure has obtained maximum value of wavelength sensitivity 16,000 nm/RIU in recently reported structures. But an internal coating method-based structure does not have advantages for real-time detection and distributed sensing purposes. It is because changing the analyte after each detection with another analyte in the air holes is a difficult and time taking task [126]. Due to such imperfections are seen in the internal sensing method, we use the second method for highly efficient sensing performances. In this method, the plasmonic layer is coated outside of the fiber, called the external sensing mechanism. In this mechanism, the analyte is in direct contact with the plasmonic layer outside of PCF [75] [127] [76]. Liu et al. obtained maximum value of wavelength sensitivity 15,180 nm/RIU with a wavelength resolution of 5.68×10^{-6} RIU for analyte range 1.40–1.43. The external sensing mechanism has become a popular sensing method due to its simple detection method with high sensing performance and a comfortable fabrication process [128]. Several structures have been proposed based on this external sensing mechanism, and it recently reported both side flat PCF structures are one of the most attractive and efficient sensing mechanisms [129] [130]. Chen et al. has obtained maximum value of wavelength sensitivity 12,400 nm/RIU with maximum value of amplitude sensitivity 252 RIU^{-1}. So researchers need to improve these results.

Chapter 3: A both side polished PCF sensor

In this study we have performed the simulation work in order to improve the sensitivity as well as sensing range than to previously reported work. Both sides flat (PCF-SPR) sensor with different size of air holes is investigated. Our main aim is to enhance sensitivity for a long analyte range. Finite element method (FEM) based COMSOL Multiphysics software have employed to simulate the proposed sensor. We have chosen an external sensing mechanism-based sensor for practical utilization and easy fabrication where the analyte channel is in direct contact with the plasmonic layer. We use gold (Au) metal as a plasmonic layer because it has chemical stability and bio-compatibility, and it provides a large resonance peak shift. An adhesive layer of TiO_2 over gold layer reinforces the interaction between analyte channel and evanescent field that shifts resonant wavelength towards the near-infrared region. We have optimized different structure parameters such as the radius of air holes, the Au layer's thickness, and the TiO_2 layer thickness to obtain desired favorable results. Peak shift of resonance wavelength and the effect on confinement loss with air hole radius, the thicknesses of the gold and the TiO_2 layers have been studied. The figure of merit (FOM) has also been calculated for the better performance of proposed sensor. This proposed structure can also be utilized in biomedical science to detect cancer cells based on their refractive index (RI).

3.2 Theoretical description

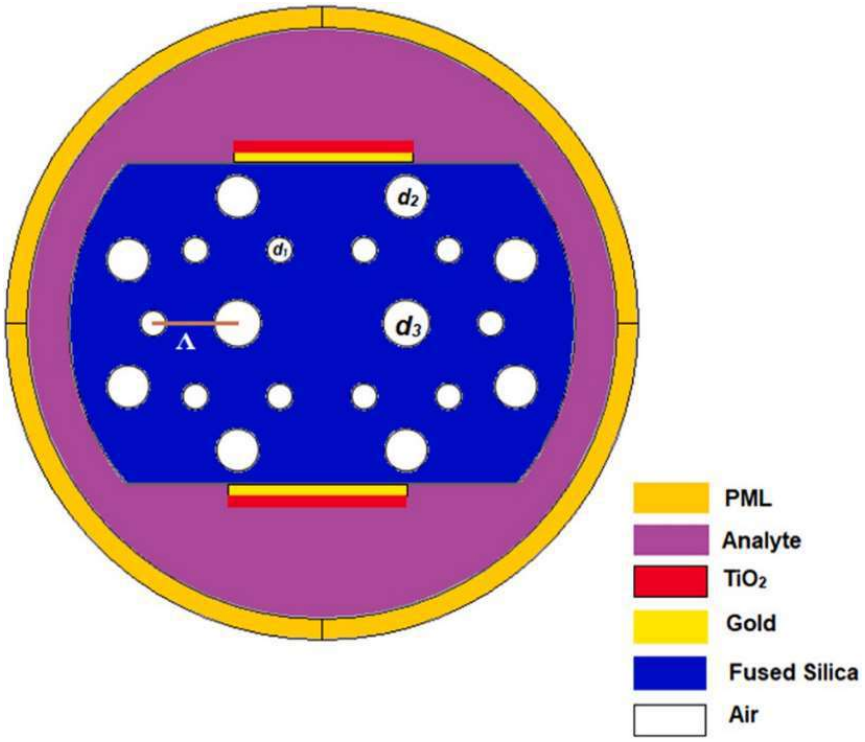

Figure 3.1 Cross-section view of propose photonic crystal fiber sensor.

The cross-section of the proposed both side flat PCF-based SPR sensor is depicted in figure 3.1. The PCF is flattened on both sides and having a hexagonal core structure with different air hole radius. The diameter of the small hole is d_1= 0.60 µm, diameter of two holes left and right side to the center of fiber is d_3 = 1.10 µm, and diameter of holes in cladding region d_2 = 1 µm and pitch (distance between two air holes) is Λ = 2 µm. The gold layer is coated on both flattened sides of PCF with an adhesive layer of TiO_2 over the gold layer that provides better interaction between the analyte channel and gold layer. The thickness of the gold metal layer and TiO_2 layer is t_g = 55 nm, t_{TiO_2} = 15 nm and the complete set-up of our proposed work has been shown in figure 3.2.

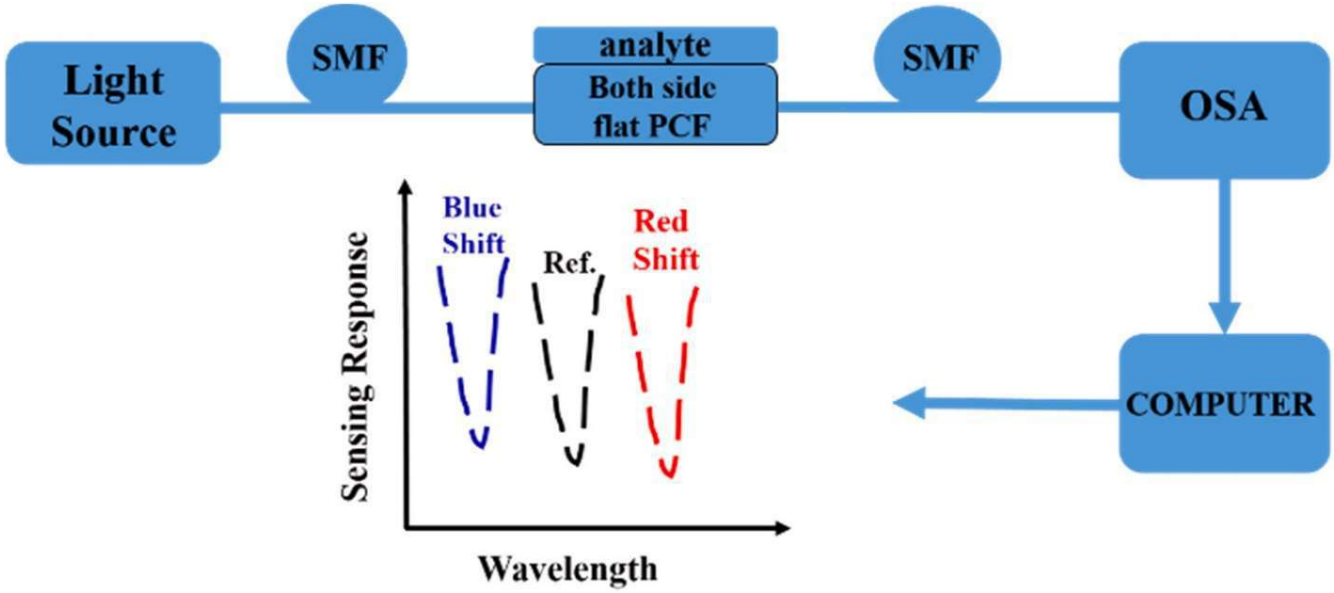

Figure 3.2 Schematic of the proposed photonic crystal fiber sensor set-up.

The background material of PCF contains fused silica whose refractive index varies with the wavelength of the incident electromagnetic wave is given by Sellmeier's equation eq. (2.1) [106]

Refractive Index (RI) of gold metal is calculated by Drude–Lorentz model given by equation [128]

$$n_{Au}^2(\lambda) = \epsilon_\infty - \frac{\omega_D^2}{\omega \times (\omega + j\Upsilon_D)} - \frac{\Delta\epsilon \times \Omega_L^2}{(\omega^2 - \Omega_L^2) + j\omega\Gamma_L} \quad (3.1)$$

where n_{Au} is the refractive index of gold (Au), and the parameters are ϵ_∞ = 5.9673 called permittivity. Angular frequency having value $\omega = \frac{2\pi c}{\lambda}$, where c = 3 × 10^8 m/s is speed of light.

Damping and plasma frequency is denoted by Υ_D and ω_D with values Υ_D = 100.03 *THz*, ω_D = 13280.14 *THz* respectively. Δϵ = 1.09 is called weighting factor and Ω_L = 4084.51 *THz*, Γ_L = 658.85 *THz* are oscillator strength and spectral width respectively of Lorentz oscillator.

Nano-layer of (TiO_2) is coated over gold layer whose RI is given by equation [131]

$$n_{TiO2}^2 = 5.913 + \frac{2.441 \times 10^7}{(\lambda^2 - 0.803 \times 10^7)} \quad (3.2)$$

Where $n_{Ti\ _2}$ refractive index of TiO_2 and λ is operating wavelength in μm.

Numerical simulation of the proposed sensor is performed on Finite Element Method (FEM) based COMSOL Multiphysics software [132]. Here, we start from Maxwell's equations and derive a set of coupled partial differential equations (PDEs) to find the longitudinal component of the electric and magnetic fields. The perfect match layer (PML) (10% thickness of fiber thickness) plays a vital role during simulation work because this PML on theoretical point of view absorbs electromagnetic wave active towards boundaries without any reflections [105]. Physics-controlled mesh using extremely fine elements has been used for higher detection accuracy. Technology is developing day by day, so fabrication of such a complex structure is also easy with the sol-gel method [133]. In this method, mold contains an array of the mandrel of required shape air holes poured in colloidal silica solution. When silica is wet, the mandrel is removed, and air holes are formed. This gel passes through a thermal process to remove contaminants, water, and other organics. The pressure is applied to air holes to provide the required size and air–filling fraction. Stack and draw is also a suitable method for PCF fabrication.

This method contains several process starting from drawing basic preform to design the final structure with required parameters such as air holes diameter (d), air hole diameter to pitch ratio (d/Λ). Ref. [100] has complete experimental procedure of stack and draw method for PCF fabrication.

Side polishing is the next task after fabricating the required PCF structure. Fiber is very small in size so it is may be a substantial task to polish it uniformly. For this support of quartz or silica block is given because they both have same material as fiber silica. We hold fiber in V-groove shape holder.

Polyurethane pads and colloidal silica slurries with an effective particle size of 0.05 μm is a single step process to polish fiber with negligible loss and effective results [134] [135] [129].

After side polishing coating of flat surface of PCF is the next step. Coating on curved surface is a bit challenging job. In order to overcome this issue researchers have chosen both sides flat PCF because coating is easy on flat surfaces compare to curved surfaces. Chemical vapor deposition (CVD) technique for film deposition is advance and better technique compare to evaporation and sputtering technique. Sample preparation and its optical measurement is done precisely in this method. Detailed explanation of its experimental work is given in this Refs. [136] [137].

3.3 Result and discussion

Electromagnetic (EM) wave launches to the core of PCF produces evanescent wave at the metal-dielectric interface is a crucial phenomenon for PCF-SPR sensor. An electron at the metal surface is excited by this evanescent wave and generates surface plasmon waves (SPWs). Light is leaked from a core-cladding arrangement that results in light launches at the metal surface to excite surface electrons.

A fixed wavelength at which the real part of effective index (n_{eff}) of core mode and real part of effective index (n_{eff}) of surface plasmon polariton (SPP) mode are equal called resonance wavelength. At this resonance wavelength, phase matching occurs to get maximum energy transfer from core guided fundamental mode to SPP mode, known as confinement loss.

For a better understanding of phase matching behavior, the dispersion profile of core guided mode, plasmonic mode, and confinement loss is represented in Fig. 3.3. In our study, we have considered a y-polarized mode of the transverse electric field (TE^y).

The plasmonic layer (gold layer) is along the y-axis direction, so the maximum amount of evanescent wave is generated along the y-axis, which results in more excitation of a free electron. The finite number of holes in the cladding region so light escaped from core of fiber to metal layer with loss of light in the core region. This loss is known as confinement loss given by the equation (1.7) [108]

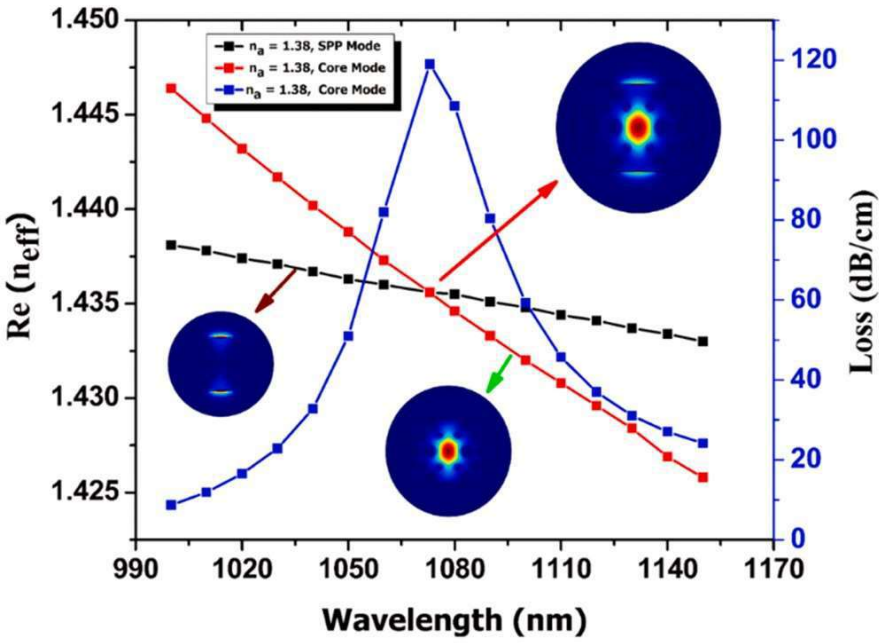

Figure 3.3 Dispersion relation of **(i)** core guided mode (red), **(ii)** plasmonic mode (black), and **(iii)** confinement loss spectrum (blue) for analyte of RI n_a= 1.38.

Analyte medium RI has a more significant impact on the real part of (n_{eff}) of plasmonic mode. A small-scale change in refractive index of the analyte medium alters the numerical value of the real part of effective index (n_{eff}) of plasmonic mode [132]. Figure 3.4. Displays the loss spectrum of analyte RI from 1.30 to 1.40. It is clear from the figure when the RI of the analyte undergoes increasing changes, and the resonant wavelength has a red-shift.

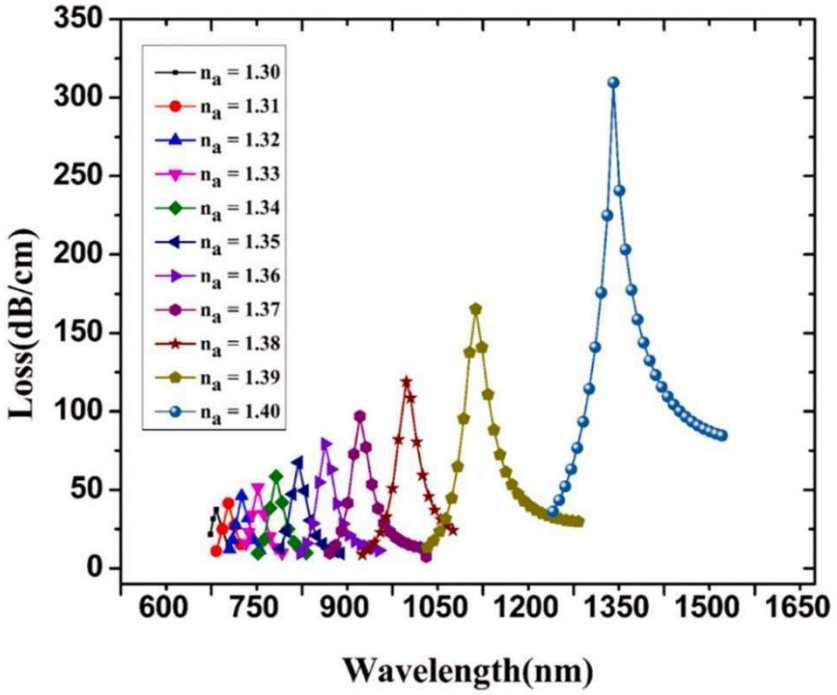

Figure 3.4 Loss spectra of analytes refractive index varies from $n_a = 1.30 - 1.40$.

PCF-based SPR sensor is very sensitive to variation of geometrical parameters. Alteration in structure parameters such as the diameter of air holes d_1, d_2, and d_3, gold metal layer thickness, the thickness of the TiO_2 layer results in a red or blue shift in resonant wavelength. Parameters of our proposed structure are d_1 = 0.60 µm, d_2 = 1.00 µm, d_3 = 1.10 µm, thickness of gold layer t_g = 55nm, and thickness of TiO_2 $t_{Ti_2} = 15\ nm$.

These PCF parameters have been chosen because variation from these selected parameters results reduction in wavelength sensitivity and amplitude sensitivity. Maximum sensitivity with a sharp loss peak is obtained with our selected parameters. Figure 3.5 (a) – (c) depicted the variation of wavelength peak with the diameter of air holes. The changing diameter d_1 from 0.60 µm to 1.00 µm resonance wavelength has a red-shift with reduced confinement loss.

This is the result of increasing the diameter coupling strength between the core-guided fundamental mode and plasmonic mode reduces, which results in reduction confinement loss. The same reduced confinement loss effect is seen while changing the diameter d_2 of the outermost air hole from 1.00 µm to 1.20 µm. Shifting diameter of core hole d_3 from 0.90–1.10 µm immunes confinement loss because having a larger hole in the core which increases the gap between holes and allows light to couple with SPP mode [138].

The thickness of the plasmonic metal layer (gold layer) has a vital role in sensor structure formation. Modulating the gold layer thickness from 55 nm to 65 nm shifts the resonance wavelength towards red-shift with less confinement loss shown in figure 3.6 (a). On increasing thickness of metal layer, penetration of electric field is less on the sensing analyte layer due to high damping loss in the metal layer [112]. So considering the high damping loss, we fix our gold layer thickness at 55 nm. Figure 3.6 (b) revealed the variation of the thickness of the TiO_2 layer. Experimental results of Tao Wang et al. [112] concluded that increasing TiO_2 layer thickness allows more penetration depth for electric field inside the sensing medium and top layer of TiO_2 over gold metal enhances its interaction to analyte channel, which results in sensitivity enhancement.

The derivative of the monitored parameter (e.g., resonance wavelength or resonance angle) with respect to parameter needs to be determined (e.g., concentration, refractive index) called the sensitivity of the SPR sensor. Here we use the wavelength interrogation method for refractive index detection, so wavelength sensitivity (S_λ) is defined by equation (2.2) [139]

The maximum wavelength sensitivity is obtained between the analyte of RI 1.39 – 1.40 with a resonance peak shift from 1188 nm to 1416 nm and average wavelength sensitivity for RI range 1.30 – 1.40 is obtained 6580 nm/RIU.

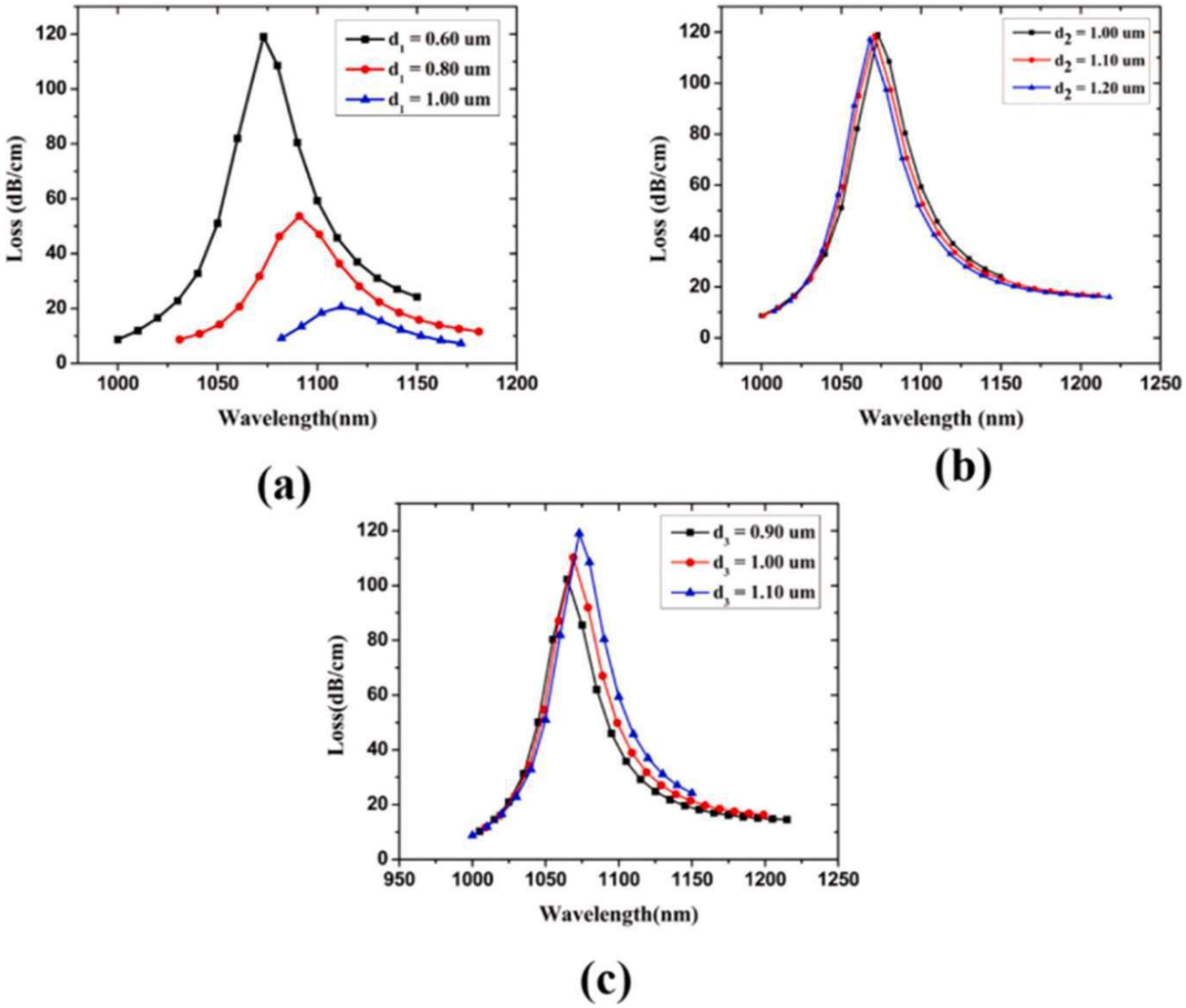

Figure 3.5 Wavelength vs. loss curve for variation of diameters **(a)** d_1, **(b)** d_2, **(c)** d_3 of proposed photonic crystal fiber sensor.

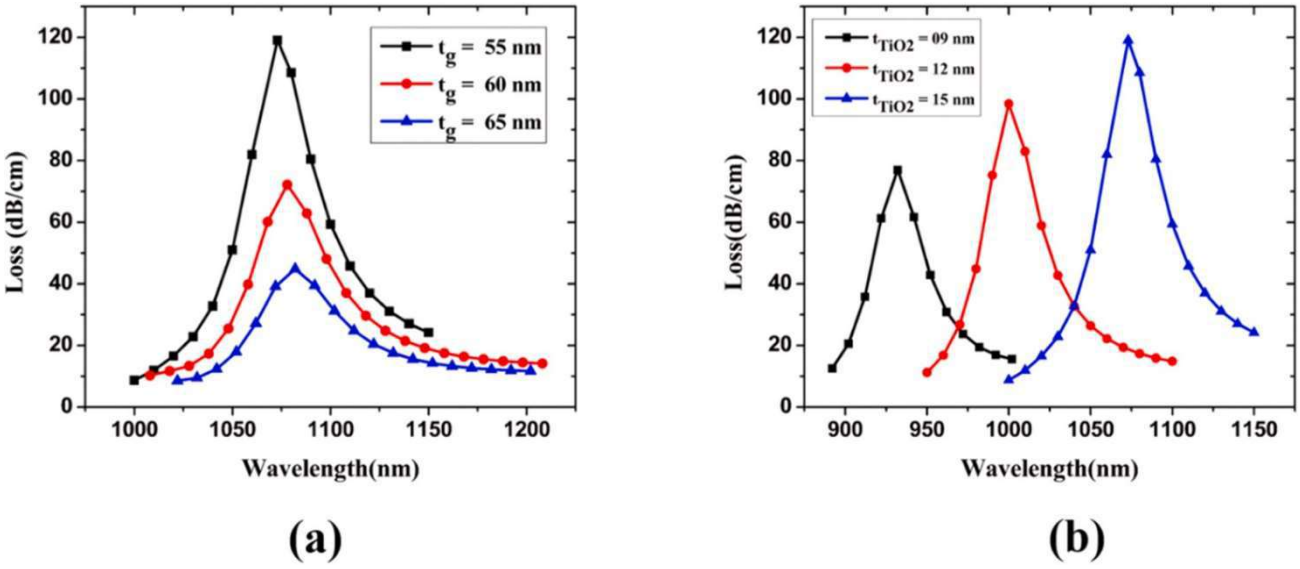

Figure 3.6 Wavelength vs. loss curve for the thickness variation of **(a)** Gold layer **(b)** TiO_2 layer.

Another method to detect RI of analyte is called the amplitude sensitivity method. In this, all operation is done at a particular wavelength so provide higher accuracy detection. It is defined by equation (2.3) [140]

The variation of amplitude sensitivity for analyte range $n_a = 1.30 - 1.39$ is depicted in figure 3.7. The value amplitude sensitivity varies with the thickness of gold layer and on increasing the value of thickness amplitude sensitivity has a down fall because of low coupling between core and SPP mode as mentioned in figure 3.8.

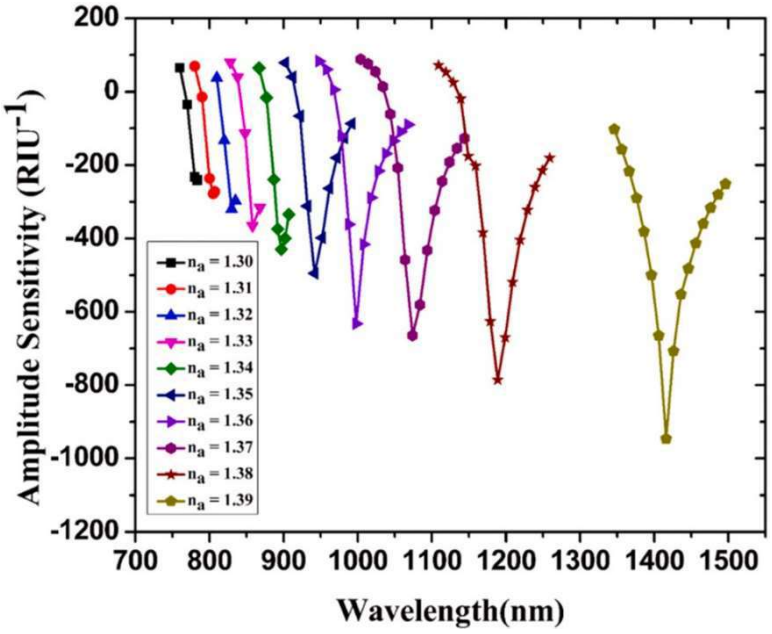

Figure 3.7 Amplitude sensitivity for analyte RI range $n_a = 1.30 - 1.39$.

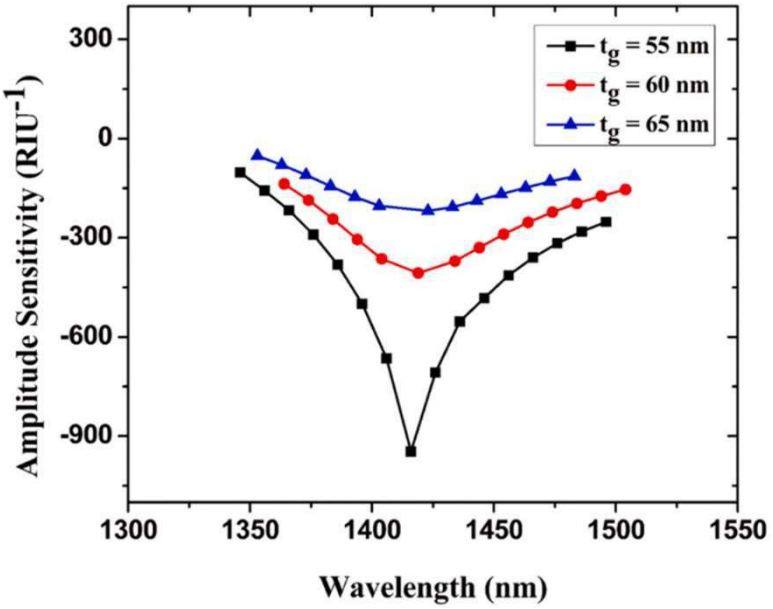

Figure 3.8 Variation of amplitude sensitivity with gold layer thickness

The minimum change in a parameter that needs to be determined by the sensor is called sensor resolution. Wavelength resolution is calculated by equation (2.4) [132].

Consider the minimum spectral resolution $\Delta\lambda_{min} = 0.1\ nm$ and a peak shift of $\Delta\lambda_{peak} = 228\ nm$ for analyte RI 1.39 – 1.40 i.e. $\Delta n_a = 0.01$. We get the maximum wavelength resolution 4.38 × 10^{-6} RIU, which means that our proposed sensor has detection accuracy upto the order of 10^{-6} for RI change measurement.

Figure of merit (FOM) is a pivotal factor to characterize the overall performance of sensor devices, and it is defined as the ratio of (S) to (FWHM) given by the following equation [112]

$$\boldsymbol{FOM = \frac{S(nm/RIU)}{FWHM\ (nm)}} \tag{3.3}$$

It is clear from the above eq. 3.3 that FOM will be high when sensitivity has a maximum value and FWHM has a minimum value. Figure 3.9 depicted the plot of FWHM vs FOM with respect to analyte RI. Our proposed structure shows the value of FWHM of 45 nm for the analyte $n_a = 1.39$, which results in FOM 507 RIU^{-1}. The value of FOM should be high in order to have high sensing performance from the PCF sensor.

The most important bio-sensing application nowadays is cancer cell detection, which has become a serious health issue in biomedical science. An easy and fast detection method should be used to detect these kinds of cells for better treatment. These cells can be detected with the help of their refractive index. Normal cells, as well as cancer cells, can be detected by our refractive index-based PCF sensor with an external sensing mechanism. Cancer cell presents in different parts of the body such as in cervical, breast, basal.

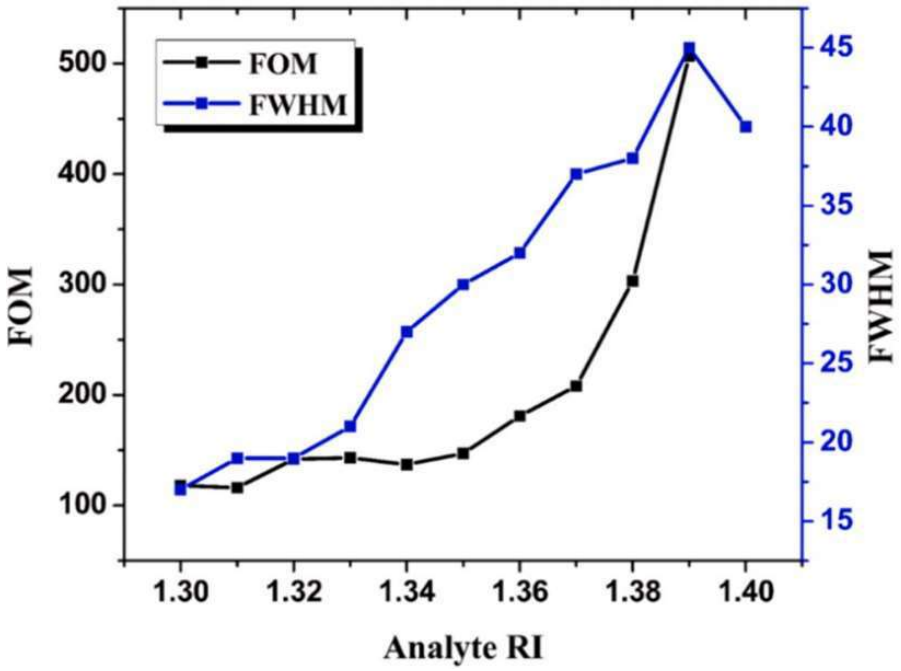

Figure 3. 9 Plot between FWHM and FOM vs. analyte RI

The sample is taken in liquid form, and the external sensing method is used because in internal sensing, filling air holes with different RI liquids is difficult and challenging task. Ayyanar et al. [59] have shown the detailed RI of normal cells and cancer cells. The refractive index of different kinds of cancer cells in different parts of body (cervical, breast, basal) mostly varies from analyte RI range 1.36–1.40 [125] and this RI range of cancer cells can easily be detected by the proposed PCF structure. Complete performance analysis of our proposed both side flat (PCF-SPR) sensor is tabulated in table 3.1.

Table 3.1 Performance of our proposed sensor structure

Analyte (RI)	Resonance Wavelength (nm)	Loss (dB/cm)	Peak shift (nm)	Wavelength Sensitivity	FWHM	FOM	Wavelength Resolution (RIU)	Amp. Sensitivity (RIU^{-1})
1.30	758	37	20	2000	17	118	5.00×10^{-5}	-243
1.31	778	41	22	2200	19	116	4.55×10^{-5}	-278
1.32	800	46	27	2700	19	142	3.70×10^{-5}	-320
1.33	827	51	30	3000	21	143	3.33×10^{-5}	-366

1.34	857	58	37	3700	27	137	2.70×10^{-5}	-430
1.35	894	67	44	4400	30	147	2.27×10^{-5}	-495
1.36	938	79	58	5800	32	181	1.72×10^{-5}	-632
1.37	996	97	77	7700	37	208	1.30×10^{-5}	-664
1.38	1073	119	115	11500	38	303	8.70×10^{-5}	-786
1.39	1188	165	228	22800	45	507	4.38×10^{-5}	-947
1.40	1416	310	---	---	40	---	---	

Figure. 3.10 introduces the polynomial fitting curve between analyte RI and resonance wavelength. Term R^2 represents a statistical measurement to determine how perfectly the data are to the fitted regression line. The value of R^2 for our proposed structure is 0.9918, which shows a better result for our sensor. A comprehensive comparison of our proposed structure with the previously reported sensor is shown in table 3.2.

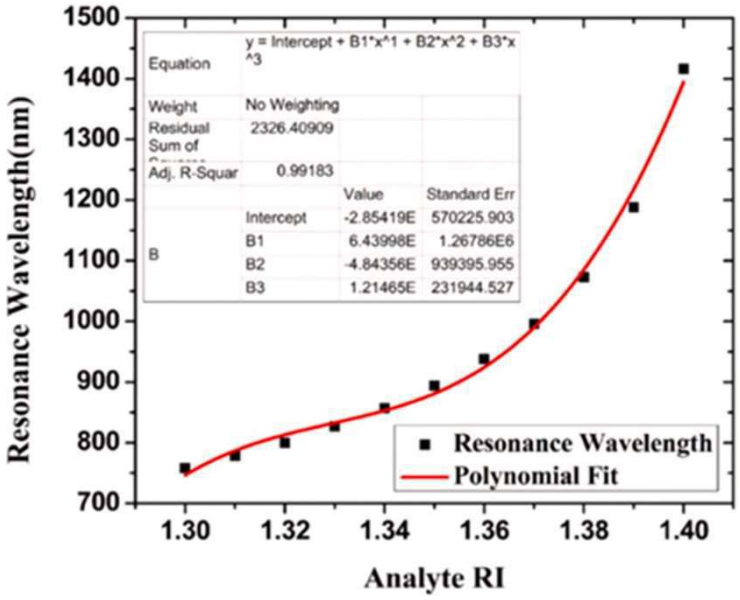

Figure 3.10 Graph of analyte RI vs. resonance wavelength

Table 3.2 Comparison of our proposed sensor structure with other available sensors solely based on simulation

References	Structure Type	RI range	Wavelength Resolution (RIU)	Wavelength Sensitivity (nm/RIU)	Amplitude Sensitivity (RIU^{-1})
[139]	Gold coating based PCF	1.34 – 1.37	1.11×10^{-5}	9000	318
[130]	Air-core PCF	1.33 – 1.41	8.55×10^{-5}	11700	160
[116]	Silver Coated PCF	1.33 – 1.37	2.38×10^{-5}	4200	300
[76]	Hexagonal PCF	1.40 – 1.43	5.68×10^{-5}	15180	498
[141]	D-Shaped PCF	1.36 – 1.38	5.98×10^{-5}	3340	70
Our Work	Both side flat PCF	1.30 – 1.40	4.38×10^{-5}	22800	947

3.4 Conclusion

In summary, both sides flat PCF sensor coated with the Gold - TiO_2 layer has been proposed in this manuscript. COMSOL Multiphysics software which is based on finite element method has been used for its design and numerical simulation. We get wavelength sensitivity of 22,800 nm/RIU and amplitude sensitivity of 947 RIU^{-1} for analyte range 1.30 – 1.40. Wavelength resolution is 4.38×10^{-6} RIU which can detect refractive index up to the order 10^{-6} and Figure of merit (FOM) is high 507 RIU^{-1} for the better limit of detection. This sensor can be very useful for cancer cells detection RI range 1.36 – 1.40 application with an external sensing approach. Nowadays, with existing new technologies, the fabrication of the proposed structure is straightforward. With these distinctive properties of our sensor, we can use it in bio-medical and chemistry for precise and high detection of bio-medicine and chemicals.